The Inhibitor DBMIB Provides Insight into the Functional Architecture of the Q_o Site in the Cytochrome b_6f Complex†

A. G. Roberts,‡,§ M. K. Bowman,‡,|| and D. M. Kramer*,‡

Institute of Biological Chemistry, Washington State University, 289 Clark Hall, Pullman, Washington 99164-6340, Structural Biology and Microimaging, Battelle Northwest Laboratories, Richland, Washington 99352-0999, and Department of Medicinal Chemistry, University of Washington, Box 357610, Seattle, Washington 98195-7610

Received March 10, 2004; Revised Manuscript Received April 16, 2004

ABSTRACT: Previously [Roberts, A. G., and Kramer, D. M. (2001) *Biochemistry 40,* 13407−13412], we showed that 2 equiv of the quinone analogue 2,5-dibromo-3-methyl-6-isopropylbenzoquinone (DBMIB) could occupy the Q_o site of the cytochrome (cyt) b_6f complex simultaneously. In this work, a study of electron paramagnetic resonance (EPR) spectra from the oriented cyt b_6f complex shows that the Rieske iron−sulfur protein (ISP) is in distinct orientations, depending on the stoichiometry of the inhibitor at the Q_o site. With a single DBMIB at the Q_o site, the ISP is oriented with the 2Fe−2S cluster toward cyt *f*, which is similar to the orientation of the ISP in the X-ray crystal structure of the cyt b_6f complex from thermophilic cyanobacterium *Mastigocladus laminosus* in the presence of DBMIB, as well as that of the chicken mitochondrial cyt bc_1 complex in the presence of the class II inhibitor myxothiazol, which binds in the so-called "proximal niche", near the cyt b_L heme. These data suggest that the high-affinity DBMIB site is at the proximal niche Q_o pocket. With ≥2 equiv of DBMIB bound, the Rieske ISP is in a position that resembles the ISP_B position of the chicken mitochondrial cyt bc_1 complex in the presence of stigmatellin and the *Chlamydomonas reinhardtii* cyt b_6f complex in the presence of tridecylstigmatellin (TDS), which suggests that the low-affinity DBMIB site is at the distal niche. The close interaction of DBMIB bound at the distal niche with the ISP induced the well-known effects on the 2Fe−2S EPR spectrum and redox potential. To further test the effects of DBMIB on the ISP, the extents of cyt *f* oxidation after flash excitation in the presence of photosystem II inhibitor DCMU were measured as a function of DBMIB concentration in thylakoids. Addition of DBMIB concentrations at which a single binding was expected did not markedly affect the extent of cyt *f* oxidation, whereas higher concentrations, at which double occupancy was expected, increased the extent of cyt *f* oxidation to levels similar to that of cyt *f* oxidation in the presence of a saturating concentration of stigmatellin. Simulations of the EPR **g**-tensor orientations of the 2Fe−2S cluster versus the physical orientations based on single-crystal studies of the cyt bc_1 complex suggest that the soluble ISP domain of the spinach cyt b_6f complex can rotate by at least 53°, which is consistent with long-range ISP domain movement. Implications of these results are discussed in the context of the X-ray crystal structures of the chicken mitochondrial cyt bc_1 complex and the *M. laminosus* and *C. reinhardtii* cyt b_6f complexes.

The cytochrome (cyt)[1] b_6f complex is the central enzyme of photosynthetic electron transport in cyanobacteria and higher-plant chloroplasts and is both functionally and structurally analogous to the mitochondrial and bacterial cyt bc_1 and *bc*-type complexes (*1*−*10*). The complex transfers electrons from plastoquinol (PQH_2) to a soluble redox carrier, plastocyanin or cyt c_6, for delivery to photosystem I. The oxidation of PQH_2 is followed by the release of protons from the stroma (n-side) to the lumen (p-side), contributing to the formation of proton motive force (pmf), which is used by the CF_1-CF_O ATP synthase to drive the synthesis of ATP.

Electron and proton transfer through the complex is thought to occur via the "Q-cycle", which was first proposed by Mitchell, and later modified by several groups (*11*−*16*). In the Q-cycle, PQH_2 is oxidized at the quinol oxidase (Q_o) site, which is formed at the interface between the cyt b_6 protein and the "head" domain, which extends into the

† This work was supported by U.S. Department of Energy Grant DE-FG03-98ER20299 and a Frasch Foundation award (D.M.K.) and NIGMS Grant GM61904 (M.K.B.). Support also was provided by the WR Wiley Environmental Molecular Sciences Laboratory, a national scientific user facility sponsored by the Department of Energy's Office of Biological and Environmental Research and located at Pacific Northwest National Laboratory.

* To whom correspondence should be addressed. Phone: ++(509) 335-4964. Fax: ++(509) 335-7643. E-mail: dkramer@wsu.edu.

‡ Washington State University.

§ Battelle Northwest Laboratories.

|| University of Washington.

[1] Abbreviations: cyt, cytochrome; DBMIB, 2,5-dibromo-3-methyl-6-isopropylbenzoquinone; DCMU, 3-(3,4-dichlorophenyl)-1,1-dimethylurea; EPR, electron paramagnetic resonance; HEPES, *N*-(2-hydroxyethyl)piperazine-*N*′-2-ethanesulfonic acid; ISP, iron−sulfur protein; pmf, proton motive force; ISP_B, iron−sulfur protein (proximal position); ISP_C, iron−sulfur protein (distal position); MOA, (*E*)-*β*-methoxyacrylate; NMR, nuclear magnetic resonance; PQ, plastoquinone; $PQ^{\bullet}$, plastosemiquinone; PQH_2, plastoquinol; Q_i, quinone reductase; Q_o, quinol oxidase; TDS, tridecylstigmatellin; UHDBT, 5-*n*-undecyl-6-hydroxy-4,7-dioxobenzothiazole; UQH_2, ubiquinol.

10.1021/bi049521f CCC: $27.50
Published on Web 05/22/2004

aqueous phase, of the "Rieske" iron−sulfur protein (ISP) (*17*, *18*). The first electron from PQH_2 is channeled through the "high-potential chain", which is comprised of the Rieske 2Fe−2S cluster in the ISP, and the cyt *f* heme in the cyt *f* subunit, forming an unstable plastosemiquinone ($PQ^{\bullet}$) and releasing two protons into the p-side of the membrane. The $PQ^{\bullet}$ is oxidized to a PQ by the "low-potential chain" consisting of cyt b_L and cyt b_H, which are ligated to the cyt b_6 subunit (*12*, *13*, *19*). Therefore, the electron transfer chain is bifurcated, with one electron going directly to the high-potential chain and the other crossing the membrane through the low-potential chain. The plastoquinone (PQ) resulting from PQH_2 oxidation at Q_o is rapidly exchanged with a PQH_2, and the process is repeated. Overall, the oxidation of PQH_2 at the Q_o site results in the release of two protons into the lumen or p-side of the membrane, and the formation of plastoquinone (PQ), which is rapidly exchanged with a PQH_2. A second turnover of the Q_o site will result in the accumulation of two electrons on the low-potential chain, which together can reduce a PQ molecule at the quinone reductase (Q_i) site, which is formed at an interface between the cyt b_6 subunit and subunit IV, to PQH_2, taking up two protons from the n-side of the membrane.

The Q-cycle is engaged over a wide range of conditions, both in vitro (*20*) and in vivo (*21*), implying that side reactions which short-circuit bifurcated electron transfer are minimized (*22*). Structural and spectroscopic studies of the cyt bc_1 complex and the cyt b_6f complex have suggested that the structure of the Q_o site and domain movement of the ISP are important for preventing the short-circuiting of bifurcated electron flow. X-ray crystal structures of the cyt bc_1 complex and the cyt b_6f complex showed that the hydrophilic head domain of the ISP is tethered by a flexible "neck" to a membrane-spanning anchor (*1*, *17*, *23*−*27*). The head domain can undergo large rotational changes with respect to the membrane-spanning anchor, depending at least on the redox state of the complex, whether inhibitors are bound at the Q_o pocket, and the crystal form (*1*, *17*, *23*−*27*). A number of different ISP positions have been identified, the extremes being the ISP_B position, which places the 2Fe−2S cluster close to the Q_o site and cyt b_L, where it can interact with Q_o site occupants (*1*, *17*, *23*), and the ISP_C position, which places the ISP near cyt c_1 or cyt *f*, where electron transfer can occur between these moieties. Intermediate positions between the ISP_B and ISP_C positions have also been identified (*28*, *29*).

When the ISP of the cyt bc_1 complex is in the ISP_C position, the 2Fe−2S cluster is close enough to allow oxidation by the cyt c_1 subunit, but is too far from the Q_o site to effectively oxidize ubiquinol. In the ISP_B position, the 2Fe−2S cluster is too far from cyt c_1 to allow oxidation of the 2Fe−2S cluster, but allows the oxidation of the ubiquinol by the 2Fe−2S cluster (*12*, *26*, *30*, *31*). Therefore, motion of the hydrophilic ISP head domain is needed to allow the 2Fe−2S cluster to interact with both the ubiquinol at the Q_o site and cyt c_1, providing a structural mechanism for bifurcation of electron flow at the Q_o site (*31*). Several groups have provided evidence for similar ISP domain movement in both the cyt bc_1 and cyt b_6f complexes (*30*, *32*−*44*).

In addition to the movement of the ISP in Q_o site catalysis, it has been previously suggested that two quinoid species (i.e., quinone, quinol, and semiquinone) may occupy the Q_o site simultaneously during turnover of the enzyme, rapidly oxidizing the reactive semiquinone and preventing the bypass reactions (*45*−*48*). Evidence of the "double-occupancy" mechanism has come from several EPR studies (*45*, *47*, *49*, *50*) and a nuclear magnetic resonance (NMR) study (*51*) of the cyt bc_1 and cyt b_6f Rieske 2Fe−2S clusters, which can be used to probe the occupancy at the Q_o site. The effects of quinones (*45*, *47*) or inhibitors (*48*−*50*, *52*) on the 2Fe−2S EPR spectra suggest the presence of a high-affinity niche and a low-affinity niche in the Q_o site to allow rapid exchange with the quinone pool (*51*, *53*). Several X-ray crystallographic and spectroscopic studies (*17*, *54*−*56*) of the cyt bc_1 complex have revealed that different classes of Q_o site inhibitors bind to two distinct niches within the Q_o site, the "distal niche" which binds inhibitors such as stigmatellin (*17*, *57*) and 5-*n*-undecyl-6-hydroxy-4,7-dioxobenzothiazole (UHDBT) (*56*, *58*) and the "proximal niche" which binds (*E*)-β-methoxyacrylate (MOA) inhibitors and myxothiazol (*17*, *59*−*61*). Other models of quinol oxidation show only one quinoid species occupying the Q_o site during catalysis that can move between the proximal and distal niches of the Q_o site (*32*) or catalyze oxidation in a concerted fashion between these niches (*60*).

The plastoquinone analogue DBMIB, which was identified as a potent inhibitor of the Q_o site (*18*), has rather interesting effects on the cyt b_6f complex. [Though most work has been done with DBMIB on the cyt b_6f complex, at least some of its effects have also been observed in cyt bc_1 complexes (*19*, *62*).] Studies using the partially oriented cyt b_6f complex show that saturating concentrations of DBMIB shift the ISP head domain orientation from one similar to that of ISP_C to one similar to that of ISP_B (*33*), which is very similar to the ISP orientation in the presence of stigmatellin (*63*). In addition, saturating concentrations of DBMIB cause a dramatic lowering of the redox midpoint potential (E_m) of the 2Fe−2S cluster (from 310 to 180 mV) (*64*), in contrast to stigmatellin and UHDBT, which cause an increase in E_m (*55*, *58*, *65*). Thermodynamically, the reduction of E_m with DBMIB binding reflects preferential binding of the inhibitor to the oxidized 2Fe−2S cluster of the ISP. We do not yet know why this is the case, but it could reflect closer pK_a matching (*66*) between hydrogen bond donors and acceptors of DBMIB [pK_a = 5.6 (*67*)] and H161 of the oxidized ISP [pK_a ∼ 7.7 and 9.0 (*68*−*70*)] versus DBMIB and H161 of the reduced ISP [pK_a = 12.5 for both protons (*71*)]. The change in redox midpoint potential is accompanied by large changes in the EPR spectrum of the reduced form, characterized by a shift in the g_y from 1.89 to 1.94 (*72*). Studies of the redox dependence of EPR spectra in the presence of excess DBMIB revealed more complex behavior, likely reflecting the interaction of the 2Fe−2S cluster with oxidized DBMIB, a bound DBMIB semiquinone species and the fully reduced hydroquinone of DBMIB (i.e., $DBMIBH_2$) (*33*, *64*). It is noteworthy that the Q-cycle is hypothesized to involve the transient production of a Q_o site semiquinone, which is thought to occur at or near the activated intermediate for the catalytic cycle (*12*, *14*).

When we looked at DBMIB binding in more detail, we found that 2 equiv of DBMIB can occupy the Q_o site simultaneously, each with distinct effects, implying two inhibitor binding sites in the Q_o pocket (*50*). The two sites

have different affinities for DBMIB, the high-affinity site, with a K_D of ~137 nM (*73*) and the low-affinity site with a K_D of 50 μM (*50*). Although the occupancy of the high-affinity site leads to inhibition of the complex, binding to the low-affinity site leads to the large changes in the EPR spectrum of the 2Fe−2S cluster (*72*−*74*).

In this work, we extend the earlier studies to show that the orientation of the ISP is differentially affected by binding of one or two DBMIB molecules in the Q_o pocket. These results have two important implications. They tell us by how much the ISP head domain can pivot, an issue not yet resolved by the X-ray structures, and where each of the DBMIB molecules likely interacts within the Q_o pocket.

MATERIALS AND METHODS

Preparation of Oriented Cyt b_6f Samples. The cyt b_6f complex was isolated from spinach thylakoids (*20*, *44*) essentially as described by Hurt and Hauska (*75*, *76*) with some modifications as described in ref *44*. Partially ordered samples were prepared from the purified cyt b_6f complex as reported previously (*63*, *77*−*80*) and with modifications in ref *44*. For oriented samples with stoichiometric amounts of DBMIB, the concentration of DBMIB was matched to the concentration of cyt *f*, as measured by the 10 mM ascrobate reduced minus 100 μM ferricyanide oxidized induced α-band at 554 nm [$\epsilon = 25$ mM^{-1} cm^{-1} (*81*)]. For oriented samples with superstoichiometric concentrations of DBMIB, the concentration of DBMIB was set to 1 mM. To minimize the amount of DBMIB reduction by ascorbate to its weak binding quinol form (*33*, *64*), samples were briefly exposed to 1 mM ascorbate and immediately frozen in liquid nitrogen, which did not appear to significantly affect the DBMIB-induced shifts in the 2Fe−2S cluster EPR spectra.

EPR Spectroscopy. Electron paramagnetic resonance spectra were obtained using a Bruker 200tt EPR spectrometer (Bruker Instruments, Billerica, MA). The sample temperature was regulated using a GFS-300 transfer tube, an ESR-900 helium cryostat, and the model ITC4 temperature controller (Oxford Instruments, Oxford, U.K.). The data were acquired using a CIO-DAS1401/12 digital I/O board (Computer Boards, Inc., Mansfield, MA) connected to a Pentium personal computer and software written in Microsoft Visual Basic version 6.0 (Microsoft, Redmond, WA). The EPR acquisition parameters are provided in the figure legends. The orientation of the Mylar sheets within the magnetic field was adjusted and measured using a Varian E-229 goniometer (Varian, Inc., Palo Alto, CA) with an accuracy of approximately ±1°. To ensure that the orientation of the 2Fe−2S cluster EPR transitions was not an artifact of sample differences in the cyt b_6f complex on the Mylar sheets, the orientation of the $g_z = 3.6$ transition of the cyt *b* hemes (*82*, *83*), whose position and orientation are highly conserved in all the X-ray crystal structures of the cyt bc_1 complex and the cyt b_6f complex that have been determined to date (*1*, *24*, *29*, *56*, *84*), was determined as described in ref *44* and found to be virtually identical in all the samples that were tested (data not shown).

*Simulation of the Orientation of the 2Fe−2S **g**-Tensor.* The EPR spectra of the oriented membrane samples were simulated in a two-step procedure, using Mathematica version 4.1 (Wolfram Research, Champaign, IL) and standard equations (*44*, *85*). A qualitative description of this method is described in ref *86*.

Structural Alignment of the Cyt bc_1 and Cyt b_6f Complexes. Using the alignment feature of DS Viewer Pro version 5.0 (Accelrys, Inc., San Diego, CA) and the cyt *b* hemes from the respective structures, the X-ray crystal structures of the chicken cyt bc_1 complex (*17*), *Chlamydomonas reinhardtii* cyt b_6f complex (*84*), and the *Mastigocladus laminosus* cyt b_6f complex (*24*) were aligned. We chose to use the cyt *b* hemes as reference because the relative positions of their irons and the heme planes change little between the cyt bc_1 and cyt b_6f complexes (*1*, *24*, *84*, *87*, *88*). The overlap between the cyt *b* hemes from the respective structures was good, with an average deviation of <1 Å, allowing us to compare the orientation of the ISPs from the respective X-ray crystal structures.

Kinetic Measurements of the Extent of Oxidation of Cyt f. Measurements were made using a flash kinetic spectrophotometer built in-house as described in ref *89* with modifications described in ref *90*. Absorbance measurements were taken at 545, 554, and 572 nm (3 nm band-pass filters at half-height), and cyt *f* redox changes were calculated as described in ref *86*. For the measurements, thylakoids (30 μg of chlorophyll/mL) in suspension buffer [50 mM *N*-(2-hydroxyethyl)piperazine-*N*′-2-ethanesulfonic acid (HEPES) (pH 7.6), 10 mM $MgCl_2$, 10 mM NaCl, and 330 mM sorbitol] with 5 μM methyl viologen, 1 μg/mL gramicidin (as an uncoupler), 10 μM 3-(3,4-dichlorophenyl)-1,1-dimethylurea (DCMU), and 1 mM ascorbate were used. The concentration of the cyt b_6f complex in the thylakoid samples was determined using the 100 μM ferricyanide minus 10 mM ascorbate reduced α-band absorbance at 554 nm of cyt *f* ($\epsilon = 25$ mM^{-1} cm^{-1}). Preparations with cyt *f* concentrations from 50 to 75 nM were used, with very similar results after normalization.

RESULTS AND DISCUSSION

The Orientation of the ISP Is Dependent on the DBMIB Stoichiometry at the Q_o Site. The physical orientation of the 2Fe−2S cluster and the soluble head domain of the ISP can be correlated to the orientation of the g_x, g_y, and g_z EPR transitions of the 2Fe−2S cluster (*33*, *44*). On the basis of pulsed EPR studies of single crystals of the cyt bc_1 complex and ligand field theory, the g_x, g_y, and g_z transitions are found roughly on the Fe−Fe axis (Fe), the axis perpendicular to a plane formed by the Fe−Fe and S−S axes (p), and the S−S (S) axis, respectively (*91*, *92*). This *g*-axis orientation was used in this work to interpret EPR data from oriented samples, allowing us to estimate the position of the ISP with respect to the membrane plane.

In one X-ray structure of the bovine cyt bc_1 complex without Q_o site occupants, the ISP was proposed in one of the structures to be in the "ISP_C" position (*28*). Using the symmetry between the cyt *b* hemes of the cyt bc_1 dimer, we generated the approximate C2 axis between the cyt bc_1 complex monomers, which should be nearly perpendicular to the membrane plane. The cyt bc_1 complex has a 2Fe−2S cluster whose Fe, p, and S axes form angles of 10.0°, 74.4°, and 11.7°, respectively, with respect to the membrane plane. The ISP in the X-ray crystal structure with the distal Q_o site occupant, stigmatellin, was proposed to be in the ISP_B position, and the 2Fe−2S cluster forms angles of ap-

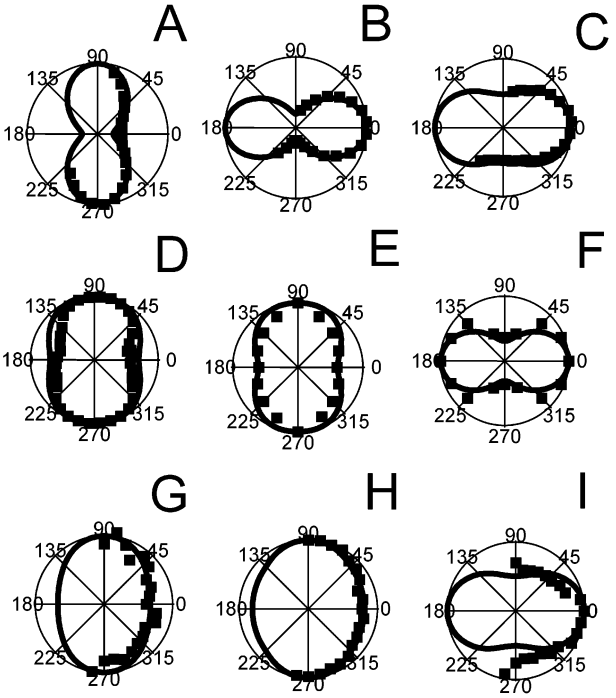

FIGURE 1: Orientation of the 2Fe−2S EPR **g**-tensor with >2 equiv of DBMIB (A−C), without inhibitors (D−F), and with 1 equiv of DBMIB (G−I). The EPR transitions are shown as follows: g_x transition in panels A, D, and G, g_y transition in panels B, E, and H, and g_z transition in panels C, F, and I. EPR spectrometer settings were as follows: microwave frequency of ~9.429 GHz, microwave power of 6.32 mW, gain of 4.0×10^5, time constant of 1000 ms, modulation amplitude of 1.6 mT, center field of 370 mT, sweep width of 200 mT, sweep time of 2 min, temperature of 20 K, and modulation frequency of 100 kHz.

proximately 80.4°, 9.2°, and 0.9° for the Fe, p, and S axes (*92*), respectively, with respect to the membrane plane. In ref *28*, an intermediate position was found for the 2Fe−2S cluster forming angles of 55.7°, 18.1°, and 27.3° for the Fe, p, and S axes, respectively, with respect to the membrane plane.

The relationship between the physical structure of the cluster and the **g**-tensor axes is known. Single-crystal EPR studies of the bovine cyt bc_1 complex in the presence of stigmatellin showed that the g_x, g_y, and g_z transitions were on average 30°, 17°, and 27°, respectively, from the physical (molecular) axes of the cluster (*86*, *92*). In the ISP_B position as defined by the cyt bc_1 complex with stigmatelin, the g_x, g_y, and g_z axes were calculated to make angles of 54.1°, 26.3°, and 22.4° with the plane of the membrane, respectively. Since the ISP_C position varies considerably between species and crystal forms (*1*, *30*), we compared the experimental **g**-tensor orientations below to the calculated **g**-tensor orientation for the ISP_B position.

Figure 1 shows the variation of the EPR signal intensity as a function of the orientation of the membrane plane in the magnetic field of the EPR spectrometer in the absence of inhibitor, with one DMBIB per cyt b_6f complex monomer, and excess DBMIB. We expected the DBMIB to be primarily in its oxidized form, since a minimum amount of ascorbate was used (see Materials and Methods), which would convert DBMIB to its weakly bound quinol form (*33*, *64*). In addition, the observed DBMIB-induced EPR transitions were consistent with the interaction of an oxidized DBMIB with the 2Fe−2S cluster of the ISP (data not shown and refs *33* and *50*). In other words, as previously observed (*33*), the line shape of the 2Fe−2S EPR signal is very different in the presence of a saturating amount of DBMIB or $DBMIBH_2$. With excess DBMIB (Figure 1A−C), the 2Fe−2S **g**-tensor axes lie 65°, 9°, and 23° from the membrane plane for the $g_x = 1.89$, $g_y = 1.94$, and $g_z = 2.01$ transitions, respectively, with a mosaic spread of ~50°, as previously observed (*33*). Although superstoichiometric amounts of DBMIB induced dramatic shifts in the 2Fe−2S EPR spectra of the cyt b_6f complex (*50*, *72*), we expected the orientation of the EPR transitions to the physical axes to be similar to those of untreated samples, since the strong nitrogen couplings of the two histidine nitrogens of the ISP in the presence of superstoichiometric DBMIB were similar to that of the uninhibited cyt b_6f complex (*93*). The calculated **g**-tensor orientation of the ISP_B position with stigmatellin (i.e., 54.1°, 26.3°, and 22.4° for the g_x, g_y, and g_z transitions, respectively, relative to the membrane plane) was relatively close to that found with excess DBMIB. This confirms the previous conclusion that the ISP is shifted into the ISP_B position by excess DBMIB (*33*).

The 2Fe−2S cluster **g**-tensor for the cyt b_6f complex without Q_o site occupants (Figure 1D−F) makes angles of 41°, 43°, and 18° from the membrane plane for the $g_x = 1.75$, $g_y = 1.89$, and $g_z = 2.03$ transitions, respectively, and a mosaic spread of ~50°, as was seen previously (*33*, *44*). The difference in the orientation of the **g**-tensor in the presence of excess DBMIB and no DBMIB is 53°, which is similar to the angle of 56° between the ISP_B and ISP_C positions of the chicken cyt bc_1 complex (*26*). Since it was shown previously that with excess DBMIB (*33*) the ISP was in the ISP_B position, the 53° displacement of the ISP in the presence of excess DBMIB and no DBMIB implies that the orientation of the ISP in the absence of DBMIB is in the ISP_C position as was previously asserted (*33*, *44*).

With 1 equiv of DBMIB, the orientation of the ISP **g**-tensor was 46°, 40°, and 16° for the $g_x = 1.745$, $g_y = 1.89$, and $g_z = 2.03$ transitions, respectively. The overall orientation was similar the orientation of the **g**-tensor for the ISP in the absence of Q_o site occupants, and is consistent with that observed in the X-ray crystal structure of the *M. laminosus* cyt b_6f complex with a singly bound DBMIB (*24*). The mosaic spread of the orientations of the 2Fe−2S cluster EPR transitions in the presence of one DBMIB was significantly increased upon binding of DBMIB, from 50° in the uninhibited control to 70°, indicating an increased heterogeneity in the orientation of the soluble head domain. The differences in mosaic spread were not artifacts of sample preparation, because the orientation of the g_z transition of cyt *b* is identical under all the conditions of this study (ref *44* and data not shown). Consistent with the higher mosaic spread, small shifts in EPR line shapes were previously observed for the g_x transition of the 2Fe−2S EPR spectrum with 1 equiv of DBMIB, shifting the g_x value of 1.740 in the uninhibited cyt b_6f complex to 1.745 (*50*).

There were strong similarities between the binding of a single DBMIB to the cyt b_6f complex and the binding of proximal Q_o site inhibitors to the cyt bc_1 complex. The cyt bc_1 complex of *Rhodobacter capsulatus* in the presence of myxothiazol also showed small shifts in the g_x transition from a g_x of 1.765 in the presence of myxothiazol to the g_x of

1.770 for quinone-extracted membranes (*45*). The orientation of the 2Fe−2S cluster **g**-tensor was similar to that in the ISP_C position, but again with significantly higher mosaic spread than uninhibited controls (*94*). This was interpreted as reflecting an increase in the number of subpositions that the ISP could adopt in the presence of the inhibitor (*94*).

Because of the similarities of proximal inhibitor binding and the high-affinity DBMIB binding, we propose that the high-affinity DBMIB site is in the proximal Q_o site niche, similar to the binding sites for other proximal niche inhibitors, e.g., myxothiazol and MOA-stilbene in the cyt bc_1 complexes (*32*, *45*, *48*). Addition of a saturating amount of DBMIB (Figure 1A−C and ref *33*) then shifts the ISP effectively into an ISP_B position, resembling the effects of distal niche inhibitors such as stigmatellin (*17*, *63*).

The Effect of DBMIB on the Extent of Cyt f Oxidation Supports the Hypothesis of Two Distinct Binding Sites within the Q_o Pocket. To test our proposal that DBMIB is both a proximal and distal niche inhibitor, we assayed the flash-induced extents of cyt *f* oxidation over a range of DBMIB concentrations. When the quinone pool is oxidized and photosystem (PS) II electron transfer is blocked by DCMU, flash excitation of P_{700} to P_{700}^+ will lead to equilibration of oxidizing equivalents among P_{700}, cyt *f*, 2Fe−2S, and PC. The extent of oxidation of these electron carriers should vary depending on the ability of the 2Fe−2S cluster to rapidly transfer electrons to cyt *f*, which in turn will be related to its position, mobility, and redox potential. When the ISP is in the ISP_C position, where it is close to cyt *f*, the ISP can equilibrate oxidizing equivalents with cyt *f*, PC, and P700. However, when the ISP is locked into the ISP_B position, where it is too far from cyt *f*, the oxidizing equivalents will remain on cyt *f*, PC, and P700, leading to a relatively higher extent of oxidation of cyt *f* and PC. Thus, the extent of oxidation of cyt *f* and PC can serve as a probe of ISP domain position. Because the cyt *f* α-band (i.e., $\lambda = 554$ nm) is relatively unobstructed by chlorophyll absorbance and the extinction coefficient is considerably higher than that of PC, we chose to look at its extent as a probe of ISP domain position. The number of flashes used to excite the samples was optimized to maximize the difference in the extents of cyt *f* oxidation between samples where the ISP was locked in the ISP_B position (i.e., with 5 μM stigmatellin) and samples where the ISP was free to move between the ISP_B and ISP_C positions (i.e., without 5 μM stigmatellin). The maximal difference in the extents of cyt *f* oxidation was observed with a train of eight saturating flashes, which only partially oxidized the cyt *f* (data not shown). Larger numbers of saturating flashes led to essentially complete photooxidation of cyt *f* in the presence of 5 μM stigmatellin (data not shown). Figure 2 shows the relative extent of cyt *f* oxidation after a train of eight saturating flashes as a function of DBMIB concentration in DCMU-treated thylakoids. To account for small differences between sample preparations, the extent of oxidation was normalized to the maximal extents of oxidation after >20 flashes in the presence of DCMU, but in the absence of cyt b_6f inhibitors.

The extent of flash train-induced cyt *f* oxidation showed a distinct sigmoidal behavior, which could be interpreted to indicate a K_D of ~5 μM. At DBMIB concentrations of >100 μM, we found significantly increased rates of cyt *f* re-reduction after the flash train, and decreased extents of oxidation, consistent with DBMIB acting as a redox mediator (*67*). The effects at higher DBMIB concentrations were insensitive to co-addition of stigmatellin, indicating that they likely did not involve the Q_o site reactions (data not shown). We were thus unable to meaningfully extend the titration to higher DBMIB concentrations. Nevertheless, the data taken over the useful concentration range, where the effects on the re-reduction rate were small, suggested that the pivoting of the ISP into the ISP_B position, where the 2Fe−2S cluster would not readily interact with cyt *f*, occurred at a DBMIB concentration well above its half-inhibitory concentration, which is in the hundreds of nanomolar (*73*). We interpret this as reflecting differences in the effects of binding of DBMIB to the high- and low-affinity sites. Binding to the high-affinity site effectively inhibits the enzyme (data not shown and refs *73* and *95*), but does not induce large changes in the ISP position, as observed in the oriented EPR data (Figure 1), and thus does not affect the equilibration of electrons between the 2Fe−2S cluster and the other carriers in the high-potential chain (Figure 2). This also implies that binding to the high-affinity site does not greatly alter the redox potential of the 2Fe−2S cluster since this would also affect the extent of flash-induced cyt *f* oxidation. On the other hand, binding to the low-affinity site forces the ISP to adopt the ISP_B position, preventing rapid equilibration with the other high-potential chain carriers. The DBMIB concentration dependence of the appearance of larger extents of cyt *f* oxidation is qualitatively consistent with the appearance of the $g = 1.94$ EPR shift in the isolated cyt b_6f complex (*50*), but with significant differences between [DBMIB] that caused the *g* shift and the elevation in the extents of cyt *f* oxidation. This discrepancy could have resulted from differences in preparation; the experiments presented here were performed with thylakoids, whereas the EPR experiments were performed with detergent-isolated, purified complexes. Alternatively, the redox mediator effects at high DBMIB concentrations may have masked part of the titration curve.

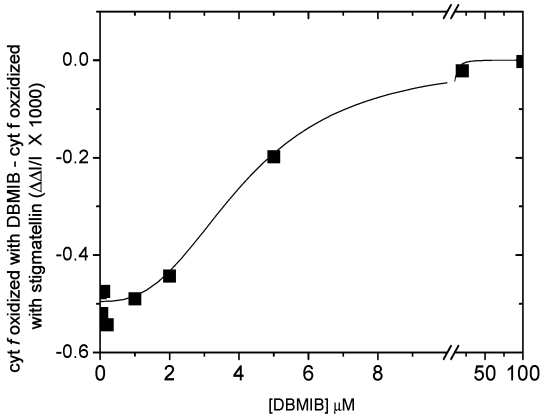

FIGURE 2: Relative extent of oxidation of cyt *f* after eight flashes as a function of DBMIB concentration in thylakoids. The extents of oxidation of cyt *f* were measured as described in Materials and Methods.

Comparison of ISP Domain Movements in the Cyt b_6f and Cyt bc_1 Complexes. It was clear from crystal structures that the ISP of the cyt bc_1 complex can undergo quite large conformational changes, with the head domain rotating about 56° (*17*, *26*). The situation with the cyt b_6f complex has been less clear. In particular, the structures of the cyt b_6f complex

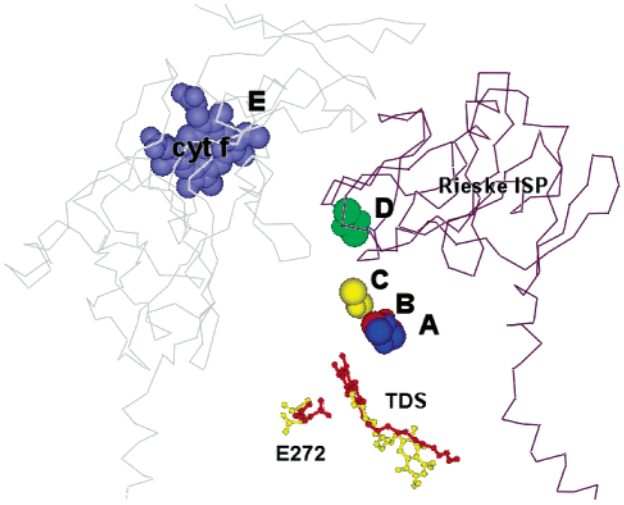

FIGURE 3: Superimposed structures of the cyt bc_1 and cyt b_6f complexes, showing the relative positions of the important structural features. (A, blue) 2Fe−2S cluster of the chicken cyt bc_1 complex in the ISP_B position in the presence of stigmatellin. (B, red) 2Fe−2S cluster, the position of tridecylstigmatellin (TDS), and E78 of cyt b_6 of the *C. reinhardtii* cyt b_6f complex. (C, yellow) 2Fe−2S cluster, the position of TDS, and E79 of cyt b_6 of the *M. laminosus* cyt b_6f complex. (D, green) 2Fe−2S cluster and (dark gray) the C_α backbone trace of the Rieske ISP of the chicken cyt bc_1 complex in the proposed ISP_C position. (E, purple) Cyt *f* heme and (light gray) the C_α backbone trace of the *M. laminosus* cyt *f* subunit.

of *M. laminosus* in the presence and absence of tridecylstigmatellin (TDS) or DBMIB suggested a rotation of only ~25° (*24*), considerably smaller than that suggested by previous EPR studies on other species (*33*, *44*, *63*). Adding to the confusion were disparate results on mutation of the region thought to act as a flexible tether, anchoring the soluble domain to the transmembrane domain between the cyt bc_1 and cyt b_6f complexes. In the cyt bc_1 complex from *Rb. capsulatus*, inserting or deleting residues in the tether region dramatically altered the activity of the enzyme as well as the conformation of the ISP (*94*, *96*). In contrast, mutations in the predicted tether region in the cyt b_6f complex from *Synechococcus* sp. PCC 7002 had comparatively little effect on the turnover and growth (*97*), suggesting either that the movements were less important or that the effects of the mutation on the tether region affected these movements less.

In this work, we confirm earlier qualitative assessments that the ISP soluble domain rotates by a large amount upon addition of a saturating amount of DBMIB (*33*). A similar extent of rotation in the presence and absence of stigmatellin could be inferred from previous EPR studies of the oriented cyt b_6f complex (*63*). Further, using numerical simulations of the EPR data (*44*) as well as estimates of the relationship between the **g**-tensor and molecular axes (*92*), we were able to give quantitative estimates of the angular positions of the ISP soluble domain under different conditions and estimate the extent of possible ISP rotation.

Figure 3 shows the positions of the 2Fe−2S cluster of the superimposed X-ray crystal structures of the cyt bc_1 and cyt b_6f complexes. In the presence of stigmatellin (Figure 3A), the 2Fe−2S cluster in the cyt bc_1 complex is in a position that is close to the cyt b_L that is known as the ISP_B position. This is virtually identical (Figure 3B) to the position of the 2Fe−2S cluster of the *C. reinhardtii* cyt b_6f complex in the presence of TDS. The orientations of TDS and E79 of cyt *b* in the *C. reinhardtii* cyt b_6f complex are also very similar to the analogous positions of stigmatellin and cyt *b* E272 of the chicken cyt bc_1 complex (*17*, *84*). In contrast, the orientation of the 2Fe−2S cluster of the *M. laminosus* cyt b_6f complex in the presence of TDS (Figure 2C) is shifted approximately 20° from the ISP_B position of the chicken cyt bc_1 complex (Figure 2A and ref *17*) or the *C. reinhardtii* cyt b_6f complex (Figure 2B and ref *84*). In addition, the headgroup of TDS is facing away from the Q_o site and the E78 (analogous to E272 of the chicken cyt bc_1 complex) is shifted away from the Q_o site (*17*), implying that the interactions of inhibitors and substrates at the Q_o site are considerably different for the *M. laminosus* cyt b_6f complex and the *C. reinhardtii* cyt b_6f complex or the chicken cyt bc_1 complex. In the absence of inhibitors or substrates, the ISP of the chicken cyt bc_1 complex in the crystal structure of Zhang and co-workers (*17*) is shifted into a position known as the ISP_C position (Figure 2D). The distance between the 2Fe−2S cluster in the ISP_C position and the iron of the cyt *f* heme is ~20 Å (*24*, *84*), which is approximately the same as the distance between the cyt c_1 iron and the 2Fe−2S cluster in the ISP_C position of the chicken cyt bc_1 complex (*17*). The C_α backbone of the ISP of the chicken cyt bc_1 complex in the ISP_C position does not overlap significantly with the C_α backbone of cyt *f* from *M. laminosus*, implying that it is possible for the soluble head domain of the ISP to occupy this position. The 2Fe−2S cluster in the ISP_C position lies ~35° from the position of the 2Fe−2S cluster of the *M. laminosus* cyt b_6f complex in the presence of TDS (Figure 3C), which is consistent with the observed 25° difference in the orientation of the soluble head domains of the ISP's in the X-ray crystal structures of the *M. laminosus* cyt b_6f complex (*24*). On the other hand, the positions of the 2Fe−2S cluster in the chicken cyt bc_1 complex in the presence of stigmatellin and in the *C. reinhardtii* cyt b_6f complex in the presence of TDS are ~55° and 57° from the ISP_C position, respectively. This implies that the angular displacement of the ISP of the *C. reinhardtii* cyt b_6f complex is considerably larger than that implied by the *M. laminosus* cyt b_6f complex, and similar to that observed in the chicken cyt bc_1 complex. This large displacement is also consistent with the displacement inferred from difference in the orientations of the EPR 2Fe−2S **g**-tensors between the spinach cyt b_6f complex in the presence of excess DBMIB and in the absence of DBMIB.

In the *M. laminosus* structure, there are no apparent hydrogen bonds between the ISP and TDS or DBMIB, and it is uncertain whether the maximum extent of ISP displacement into the ISP_C position had been achieved. In fact, the small apparent angular displacement of the thermophilic cyanobacterial, *M. laminosus*, cyt b_6f complex could represent increased "stiffness" in the ISP tether, as an adaptation to a higher growth temperature [i.e., 45−55 °C (*98*)].

A Model of Two DBMIBs in the Q_o Site and Its Relationship to Q_o Site Catalysis. Scheme 1 shows the proposed orientation of the DBMIB molecules in the hypothetical Q_o site pocket of the cyt b_6f complex, using the highly conserved structural features from the X-ray crystal structure of the chicken cyt bc_1 complex and *C. reinhardtii* cyt b_6f complex (*17*, *84*). Kinetic and orientation data support binding of the first (tightly bound) DBMIB to the Q_o site in a fashion that

Scheme 1: Ball-and-Stick Model of the Q_o Site Showing the Hypothetical Positions of Two DBMIBs in the Q_o Site Pocket[a]

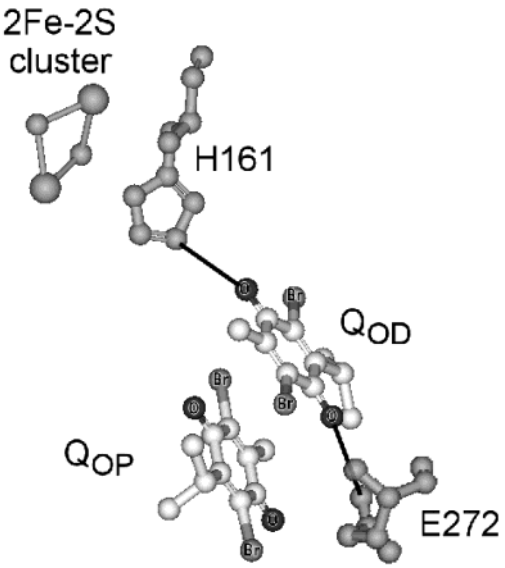

[a] Within the Q_o site, E272 of cyt *b*, the 2Fe−2S cluster, and H161 of the Rieske ISP are shown, using chicken cyt bc_1 complex numbering (*17*, *84*). The labels O and Br denote the positions of the oxygen and bromine atoms on DBMIB, respectively. The first tightly bound DBMIB is bound at the proximal niche, while the weakly bound DBMIB is bound at the distal niche. The weakly bound DBMIB is hydrogen bonded to the carboxylate side group of E272 on cyt *b* (black line) and Nϵ of H161 on the ISP.

is similar to that of the proximal Q_o site inhibitors, myxothiazol and MOA-stilbene (*17*). We show this DBMIB to be in the proximal niche of the Q_o site in a position similar to that of myxothiazol or MOA-stilbene in the X-ray crystal structures of the chicken cyt bc_1 complex (*17*). This is also consistent with the position of the single DBMIB bound at the Q_o pocket in the *M. laminosus* complex (*24*).

In the presence of superstoichiometric concentrations of DBMIB, our data support binding of a second (less tightly bound) DBMIB in the Q_o site pocket, similar to the case for the distal Q_o site inhibitors, stigmatellin and UHDBT. The DBMIB should be bound to the distal niche of the Q_o site in a fashion similar to that of stigmatellin in the X-ray structure of the chicken cyt bc_1 complex (*17*). One oxygen atom from a quinone ketone group forms a hydrogen bond with ϵ-N of the Rieske ISP H161 and the carboxylate side group of the cyt *b* E272 for the chicken cyt bc_1 complex or E79 for the *C. reinhardtii* cyt b_6f complex. The close interaction of the DBMIB with H161 of the ISP is consistent with the large effects of binding of the second DBMIB on the 2Fe−2S EPR spectrum, as well as the suggested strong spin coupling of DBMIB semiquinone with the 2Fe−2S center (*33*, *64*).

Implications for Substrate, Intermediate, and Product Binding Properties of the Q_o Pocket. Because DBMIB is structurally similar to the substrate PQ, it is reasonable to suggest that its binding may at least partly mimic that of the substrate, and perhaps that of some intermediate species. Similar arguments were made for the binding of stigmatellin (*17*, *61*). We have previously presented evidence that two molecules of DBMIB bind to the Q_o pocket (*50*). The current work suggests that the high-affinity site is similar to the so-called proximal niche, as found, for example, for myxothiazol or MOA-stilbene bound to cyt bc_1 complexes, or DBMIB bound to the *M. laminosus* b_6f complex. The low-affinity site, on the other hand, is similar to the so-called distal niche, typified by stigmatellin in both cyt bc_1 (*17*) and the *C. reinhardtii* cyt b_6f structure (*84*). These suggested assignments are strikingly similar for the Q_{os} and Q_{ow} binding sites (for the strong and weak Q_o binding sites, respectively) proposed by Dutton and co-workers in their double-occupancy models (*47*, *48*).

Our finding of two DBMIB sites also reconciles the single DBMIB-containing crystal structure of *M. laminosus* with what has been previously reported about the action of DBMIB (*24*), i.e., that it strongly influences both the redox potential and the EPR spectrum of the 2Fe−2S cluster (*64*). Indeed, we found that there is nothing sterically preventing the soluble head domain from assuming the ISP_B position (see ref *24* and data not shown). Since the Q_o site of *M. laminosus* appears to bind to TDS in a manner quite distinct from that of the Q_o site of the *C. reinhardtii* cyt b_6f complex, this would suggest that the binding of DBMIB to the Q_o site of *M. laminosus* might also be distinct (*24*, *84*).

Moreover, the binding of DBMIB at the Q_o site and the similarities in the rotation of the soluble ISP head domain between the ISP_B and ISP_C positions between the cyt b_6f and cyt bc_1 complexes (with the possible exception of the *M. laminosus* system) imply that the mechanisms of catalysis and the structure of the Q_o site for the cyt b_6f and cyt bc_1 complexes are highly conserved, despite substantial differences in the tertiary structures of the complexes (*1*, *17*, *24*, *84*). This supports previous views (*1*, *24*) that ISP domain movements are a key part of cyt bc_1 and cyt b_6f catalysis, and further suggests that any large evolutionary changes in the structure of the complexes were offset to allow the ISP domain movements to continue.

ACKNOWLEDGMENT

We thank Drs. Jason Cooley, Fevzi Daldal, and William Cramer for important discussions.

REFERENCES

1. Berry, E. A., Guergova-Kuras, M., Huang, L., and Crofts, A. R. (2000) Structure and function of cytochrome *bc* complexes, *Annu. Rev. Biochem. 69*, 1005−1075.
2. Cramer, W. A., Martinez, S. E., Huang, D., Tae, G.-S., Everly, R. M., Heymann, J. B., Cheng, R. H., Baker, T. S., and Smith, J. L. (1994) Structural aspects of the cytochrome b_6f complex; structure of the lumen-side domain of cytochrome *f*, *J. Bioenerg. Biomembr. 26*, 31−47.
3. Soriano, G. M., Ponamarev, M. V., Carrell, C. J., Xia, D., Smith, J. L., and Cramer, W. A. (1999) Comparison of the cytochrome bc_1 complex with the anticipated structure of the b_6f complex: de plus ca change de ples c'est la meme chose, *J. Bioenerg. Biomembr. 31*, 201−213.
4. Hope, A. B. (2000) Electron transfers amongst cytochrome *f*, plastocyanin and photosystem I: kinetics and mechanisms, *Biochim. Biophys. Acta 1456*, 5−26.
5. Trumpower, B. L., and Gennis, R. B. (1994) Energy transduction by cytochrome complexes in mitochondrial and bacterial respiration: the enzymology of coupling electron-transfer reactions to transmembrane proton translocation, *Annu. Rev. Biochem. 63*, 675−716.
6. Sone, N., Tsuchiya, N., Inoue, M., and Noguchi, S. (1996) *Bacillus stearothermophilus* qcr operon encoding Rieske FeS protein, cytochrome b_6, and a novel-type cytochrome c_1 of quinol-cytochrome *c* reductase, *J. Biol. Chem. 271*, 12457−12462.
7. Yu, J., and Le Brun, N. E. (1998) Studies of the cytochrome subunits of menaquinone:cytochrome *c* reductase (*bc* complex)

of *Bacillus subtilis*. Evidence for the covalent attachment of heme to the cytochrome *b* subunit, *J. Biol. Chem. 273*, 8860−8866.
8. Hauska, G., Schutz, M., and Buttner, M. (1996) The cytochrome b_6f complex-composition structure and function, in *Oxygenic Photosynthesis: The Light Reactions* (Ort, D. R., and Yocum, C. F., Eds.) pp 377−398, Kluwer Academic Publishers, Dordrecht, The Netherlands.
9. Kallas, T. (1994) The cytochrome b_6f complex, in *The Molecular Biology of Cyanobacteria* (Bryant, D. A., Ed.) pp 259−317, Kluwer Academic Publishers, Dordrecht, The Netherlands.
10. Mosser, G., Breyton, C., Olofsson, A., Popot, J. L., and Rigaud, J. L. (1997) Projection map of cytochrome b_6f complex at 8 Å resolution, *J. Biol. Chem. 272*, 20263−20268.
11. Mitchell, P. (1975) The protonmotive Q cycle: a general formulation, *FEBS Lett. 59*, 137−139.
12. Crofts, A. R., and Wang, Z. (1989) How rapid are the internal reactions of the ubiquinol:cytochrome c_2 oxidoreductase? *Photosynth. Res. 22*, 69−87.
13. Trumpower, B. L. (1990) The protomotive Q cycle: energy transduction by coupling of proton translocation to electron transfer by the cytochrome bc_1 complex, *J. Biol. Chem. 265*, 11409−11412.
14. Crofts, A. R. (1985) The mechanism of the ubiquinol: cytochrome *c* oxidoreductases of mitochondria and of *Rhodopseudomonas sphaeroides*, in *The Enzymes of Biological Membranes* (Martonosi, A. N., Ed.) pp 347−382, Plenum Publishing, New York.
15. Brandt, U., and Trumpower, B. (1994) The protonmotive Q cycle in mitochondria and bacteria, *Crit. Rev. Biochem. Mol. Biol. 29*, 165−197.
16. Brandt, U. (1996) Bifurcated ubihydroquinone oxidation in the cytochrome bc_1 complex by proton-gated charge transfer, *FEBS Lett. 387*, 1−6.
17. Zhang, Z., Huang, L., Shulmeister, V. M., Chi, Y. I., Kim, K. K., Hung, L. W., Crofts, A. R., Berry, E. A., and Kim, S. H. (1998) Electron transfer by domain movement in cytochrome bc_1, *Nature 392*, 677−684.
18. Chain, R. K., and Malkin, R. (1979) On the interaction of 2,5-dibromo-3-methyl-6-isopropylbenzoquinone (DBMIB) with bound electron carriers in spinach chloroplasts, *Arch. Biochem. Biophys. 197*, 52−56.
19. Rich, P. R. (1984) Electron and proton transfers through quinones and cytochrome *bc* complexes, *Biochim. Biophys. Acta 768*, 53−79.
20. Kramer, D. M., and Crofts, A. R. (1993) The concerted reduction of the high- and low-potential chains of the *bf* complex by plastoquinol, *Biochim. Biophys. Acta 1183*, 72−84.
21. Sacksteder, C. A., Kanazawa, A., Jacoby, M. E., and Kramer, D. M. (2000) The proton to electron stoichiometry of steady-state photosynthesis in living plants: A proton-pumping Q cycle is continuously engaged, *Proc. Natl. Acad. Sci. U.S.A. 97*, 14283−14288.
22. Muller, F., Crofts, A. R., and Kramer, D. M. (2002) Multiple Q-cycle bypass reactions at the Q_o site of the cytochrome bc_1 complex, *Biochemistry 41*, 7866−7874.
23. Crofts, A. R., Berry, E. A., Kuras, R., Guergova-Kuras, M., Hong, S., and Ugulava, N. B. (1999) Structures of the bc_1 complex reveal dynamic aspects of mechanism, in *Photosynthesis: Mechanisms and Effects* (Garab, G., Ed.) pp 1481−1486, Kluwer Academic Publishers, Dordrecht, The Netherlands.
24. Kurisu, G., Zhang, H., Smith, J. L., and Cramer, W. A. (2003) Structure of the cytochrome b_6f complex of oxygenic photosynthesis: tuning the cavity, *Science 302*, 1009−1014.
25. Xia, D., Yu, C. A., Kim, H., Xia, J. Z., Kachurin, A. M., Zhang, L., Yu, L., and Deisenhofer, J. (1997) Crystal structure of the cytochrome bc_1 complex from bovine heart mitochondria, *Science 277*, 60−66.
26. Izrailev, S., Crofts, A. R., Berry, E. A., and Schulten, K. (1999) Steered molecular dynamics simulation of the Rieske subunit motion in the cytochrome bc_1 complex, *Biophys. J. 77*, 1753−1768.
27. Darrouzet, E., Moser, C. C., Dutton, P. L., and Daldal, F. (2001) Large scale domain movement in cytochrome bc_1: a new device for electron transfer in proteins, *Trends Biochem. Sci. 26*, 445−451.
28. Iwata, S., Lee, J. W., Okada, K., Lee, J. K., Iwata, M., Rasmussen, B., Link, T. A., Ramaswamy, S., and Jap, B. K. (1998) Complete structure of the 11-subunit bovine mitochondrial cytochrome bc_1 complex, *Science 281*, 64−71.
29. Hunte, C., Koepke, J., Lange, C., Rossmanith, T., and Michel, H. (2000) Structure at 2.3 Å resolution of the cytochrome bc_1 complex from the yeast *Saccharomyces cerevisiae* cocrystallized with an antibody Fv fragment, *Struct. Folding Des. 8*, 669−684.
30. Crofts, A. R., Guergova-Kuras, M., Huang, L., Kuras, R., Zhang, Z., and Berry, E. A. (1999) Mechanism of ubiquinol oxidation by the bc_1 complex: role of the iron sulfur protein and its mobility, *Biochemistry 38*, 15791−15806.
31. Crofts, A. R., Hong, S., Zhang, Z., and Berry, E. A. (1999) Physicochemical aspects of the movement of the Rieske iron sulfur protein during quinol oxidation by the bc_1 complex from mitochondria and photosynthetic bacteria, *Biochemistry 38*, 15827−15839.
32. Brugna, M., Rodgers, S., Schricker, A., Montoya, G., Kazmeier, M., Nitschke, W., and Sinning, I. (2000) A spectroscopic method for observing the domain movement of the Rieske iron−sulfur protein, *Proc. Natl. Acad. Sci. U.S.A. 97*, 2069−2074.
33. Schoepp, B., Brugna, M., Riedel, A., Nitschke, W., and Kramer, D. M. (1999) The Q_o-site inhibitor DBMIB favours the proximal position of the chloroplast Rieske protein and induces a p*K*-shift of the redox-linked proton, *FEBS Lett. 450*, 245−250.
34. Brugna, M., Nitschke, W., Asso, M., Guigliarelli, B., Lemesle-Meunier, D., and Schmidt, C. (1999) Redox components of cytochrome *bc*-type enzymes in acidophilic prokaryotes. II. The Rieske protein of phylogenetically distant acidophilic organisms, *J. Biol. Chem. 274*, 16766−16772.
35. Liebl, U., Pezennec, S., Riedel, A., Kellner, E., and Nitschke, W. (1992) The Rieske FeS center from the Gram-positive bacterium PS3 and its interaction with the menaquinone pool studied by EPR, *J. Biol. Chem. 267*, 14068−14072.
36. Breyton, C. (2000) Conformational changes in the cytochrome b_6f complex induced by inhibitor binding, *J. Biol. Chem. 275*, 13195−13201.
37. Heimann, S., Ponamarev, M. V., and Cramer, W. A. (2000) Movement of the Rieske iron−sulfur protein in the *p*-side bulk aqueous phase: Effect of lumenal viscosity on redox reactions of the cytochrome b_6f complex, *Biochemistry 39*, 2692−2699.
38. Xiao, K., Yu, L., and Yu, C. A. (2000) Confirmation of the involvement of protein domain movement during the catalytic cycle of the cytochrome bc_1 complex by the formation of an intersubunit disulfide bond between cytochrome *b* and the iron−sulfur protein, *J. Biol. Chem. 275*, 38597−38604.
39. Darrouzet, E., Valkova-Valchanova, M., Moser, C. C., Dutton, P. L., and Daldal, F. (2000) Uncovering the [2Fe2S] domain movement in cytochrome bc_1 and its implications for energy conversion, *Proc. Natl. Acad. Sci. U.S.A. 97*, 4567−4572.
40. Darrouzet, E., Valkova-Valchanova, M., Ohnishi, T., and Daldal, F. (1999) Structure and function of the bacterial bc_1 complex: domain movement, subunit interactions, and emerging rationale engineering attempts, *J. Bioenerg. Biomembr. 31*, 275−288.
41. Nett, J. H., Hunte, C., and Trumpower, B. L. (2000) Changes to the length of the flexible linker region of the Rieske protein impair the interaction of ubiquinol with the cytochrome bc_1 complex, *Eur. J. Biochem. 267*, 5777−5782.
42. Valkova-Valchanova, M., Darrouzet, E., Moomaw, C. R., Slaughter, C. A., and Daldal, F. (2000) Proteolytic cleavage of the Fe−S subunit hinge region of *Rhodobacter capsulatus* bc_1 complex: effects of inhibitors and mutations, *Biochemistry 39*, 15484−15492.
43. Rao, S. R. B., Tyryshkin, A. M., Roberts, A. G., Bowman, M. K., and Kramer, D. M. (2000) Inhibitory copper binding site on the spinach cytochrome b_6f complex: implications for Q_o site catalysis, *Biochemistry 39*, 3285−3296.
44. Roberts, A. G., Bowman, M. K., and Kramer, D. M. (2002) Certain metal ions are inhibitors of cytochrome b_6f complex 'Rieske' iron−sulfur protein domain movements, *Biochemistry 41*, 4070−4079.
45. Ding, H., Robertson, D. E., Daldal, F., and Dutton, P. L. (1992) Cytochrome bc_1 complex [2Fe-2S] cluster and its interaction with ubiquinone and ubihyroquinone at the Q_o site: a double-occupancy Q_o site model, *Biochemistry 31*, 3144−3158.
46. Brandt, U. (1996) Energy conservation by bifurcated electron-transfer in the cytochrome-bc_1 complex, *Biochim. Biophys. Acta 1275*, 41−46.
47. Ding, H., Moser, C. C., Robertson, D. E., Tokito, M. K., Daldal, F., and Dutton, P. L. (1995) Ubiquinone pair in the Q_o site central to the primary energy conversion reactions of cytochrome bc_1 complex, *Biochemistry 34*, 15979−15996.

48. Sharp, R. E., Moser, C. C., Gibney, B. R., and Dutton, P. L. (1999) Primary steps in the energy conversion reaction of the cytochrome bc_1 complex Q_o site, *J. Bioenerg. Biomembr. 31*, 225−233.
49. Sharp, R. E., Gibney, B. R., Palmitessa, A., White, J. L., Dixon, J. A., Moser, C. C., Daldal, F., and Dutton, P. L. (1999) Effect of inhibitors on the ubiquinone binding capacity of the primary energy conversion site in the *Rhodobacter capsulatus* cytochrome bc_1 complex, *Biochemistry 38*, 14973−14980.
50. Roberts, A. G., and Kramer, D. M. (2001) Inhibitor 'double-occupancy' in the Q_o pocket of the chloroplast cytochrome b_6f complex, *Biochemistry 40*, 13407−13412.
51. Bartoschek, S., Johansson, M., Geierstanger, B. H., Okun, J. G., Lancaster, C. R., Humpfer, E., Yu, L., Yu, C. A., Griesinger, C., and Brandt, U. (2001) Three molecules of ubiquinone bind specifically to mitochondrial cytochrome bc_1 complex, *J. Biol. Chem. 276*, 35231−35234.
52. Matsuura, K., Bowyer, J. R., Ohnishi, T., and Dutton, P. L. (1983) Inhibition of electron transfer by 3-alkyl-2-hydroxy-1,4-naphthoquinones in the ubiquinol-cytochrome *c* oxidoreductases of *Rhodopseudomonas sphaeroides* and mammalian mitochondria, *J. Biol. Chem. 258*, 1571−1579.
53. Sharp, R. E., Palmitessa, A., Gibney, B. R., White, J. L., Moser, C. C., Daldal, F., and Dutton, P. L. (1999) Ubiquinone binding capacity of the *Rhodobacter capsulatus* cytochrome bc_1 complex: effect of diphenylamine, a weak binding Q_o site inhibitor, *Biochemistry 38*, 3440−3446.
54. Brandt, U., Schagger, H., and von Jagow, G. (1988) Characterisation of binding of the methoxyacrylate inhibitors to mitochondrial cytochrome *c* reductase, *Eur. J. Biochem. 173*, 499−506.
55. von Jagow, G., and Ohnishi, T. (1985) The chromone inhibitor stigmatellin-binding to the ubiquinol oxidation center at the *c*-side of the mitochondrial membrane, *FEBS Lett. 185*, 311−315.
56. Palsdottir, H., Lojero, C. G., Trumpower, B. L., and Hunte, C. (2003) Structure of the yeast cytochrome bc_1 complex with a hydroxyquinone anion Q_o site inhibitor bound, *J. Biol. Chem. 278*, 31303−31311.
57. Ohnishi, T., Brandt, U., and von Jagow, G. (1988) Studies on the effect of stigmatellin derivatives on cytochrome *b* and the Rieske iron−sulfur cluster of cytochrome *c* reductase from bovine heart mitochondria, *Eur. J. Biochem. 176*, 385−389.
58. Bowyer, J. R., and Trumpower, B. L. (1980) Inhibition of the oxidant-induced reduction of cytochrome *b* by a synthetic analogue of ubiquinone, *FEBS Lett. 115*, 171−174.
59. Link, T. A., Haase, U., Brandt, U., and Jagow, G. v. (1993) What information do inhibitors provide about the structure of hydroquinone oxidation site of ubihydroquinone: cytochrome *c* oxidoreductase? *J. Bioenerg. Biomembr. 25*, 221−232.
60. Rich, P. R., Madgwick, S. A., Brown, S., von Jagow, G., and Brandt, U. (1992) MOA-stilbene: a new tool for investigation of the reactions of the chloroplast cytochrome *bf* complex, *Photosynth. Res. 34*, 465−477.
61. Muller, F. L., Roberts, A. G., Bowman, M. K., and Kramer, D. M. (2003) The architecture of the Q_o site of the cytochrome bc_1 complex probed by superoxide production, *Biochemistry 42*, 6493−6499.
62. Loschen, G., and Azzi, A. (1974) Dibromothymoquinone: a new inhibitor of mitochondrial electron transport at the level of ubiquinone, *FEBS Lett. 41*, 115−117.
63. Riedel, A., Rutherford, A. W., Hauska, G., Muller, A., and Nitschke, W. (1991) Chloroplast Rieske center. EPR study on its spectral characteristics, relaxation and orientation properties, *J. Biol. Chem. 266*, 17838−17844.
64. Malkin, R. (1981) Redox properties of the DBMIB−Rieske iron−sulfur complex in spinach chloroplast membranes, *FEBS Lett. 131*, 169−172.
65. Oettmeier, W., Godde, D., Kunze, B., and Hofle, G. (1985) Stigmatellin. A dual type inhibitor of photosynthetic electron transport, *Biochim. Biophys. Acta 807*, 216−219.
66. Schwartz, B., Drueckhammer, D. G., Usher, K. C., and Remington, S. J. (1995) α-Fluoro acid and α-fluoro amide analogs of acetyl-CoA as inhibitors of citrate synthase: effect of pK_a matching on binding affinity and hydrogen bond length, *Biochemistry 34*, 15459−15466.
67. Prince, R. C., Linkletter, S. J. G., and Dutton, P. L. (1981) The thermodynamic properties of some commonly used oxidation−reduction mediators, inhibitors and dyes, as determined by polarography, *Biochim. Biophys. Acta 635*, 132−148.
68. Link, T. A. (1994) Two p*K* values of the oxidized 'Rieske' [2Fe-2S] cluster observed by CD spectroscopy, *Biochim. Biophys. Acta 1185*, 81−84.
69. Kuila, D., and Fee, J. A. (1986) Evidence for a redox-linked ionizable group associated with the [2Fe-2S] cluster of *Thermus* Rieske protein, *J. Biol. Chem. 261*, 2768−2771.
70. Prince, R. C., and Dutton, P. L. (1976) Furthur studies on the Rieske iron−sulfur center in mitochondrial and photosynthetic systems: A p*K* on the oxidized form, *FEBS Lett. 65*, 117−119.
71. Zu, Y., Fee, J. A., and Hirst, J. (2001) Complete thermodynamic characterization of reduction and protonation of the bc_1-type Rieske [2Fe-2S] center of *Thermus thermophilus*, *J. Am. Chem. Soc. 123*, 9906−9907.
72. Malkin, R. (1981) Interaction of the quinone analogue, DBMIB, with the photosynthetic Rieske iron−sulfur center, *Isr. J. Chem. 21*, 301−305.
73. Oettmeier, W., Masson, K., and Dostatni, R. (1987) Halogenated 1,4-benzoquinones as irreversibly binding inhibitors of photosynthetic electron transport, *Biochim. Biophys. Acta 890*, 260−269.
74. Lozier, R. H., and Butler, W. L. (1972) The effects of dibromothymoquinone on fluorescence and electron transport of spinach chloroplasts, *FEBS Lett. 26*, 161−164.
75. Hurt, E., and Hauska, G. (1981) A cytochrome f/b_6 complex of five polypeptides with plastoquinol-plastocyanin-oxidoreductase activity from spinach chloroplasts, *Eur. J. Biochem. 117*, 591−599.
76. Hauska, G. (1986) Preparations of electrogenic, proton-transporting cytochrome complexes of the b_6f-type (chloroplasts and cyanobacteria) and bc_1-type (*Rhodopseudomonas sphaeroides*), *Methods Enzymol. 126*, 271−285.
77. Rutherford, A. W., and Setif, P. (1990) Orientation of P700, the primary electron donor of photosystem I, *Biochim. Biophys. Acta 1019*, 128−132.
78. Blasie, J. K., Erecinska, M., Samuels, S., and Leigh, J. S. (1978) The structure of a cytochrome oxidase-lipid model membrane, *Biochim. Biophys. Acta 501*, 33−52.
79. More, C., Belle, V., Asso, M., Fournel, A., Roger, G., and Guigliarelli, B. (1999) EPR spectroscopy: a powerful technique for the structural and functional investigation of metalloproteins, *Biospectroscopy 5*, S3−S18.
80. Guigliarelli, B., Guillaussier, J., More, C., Setif, P., Bottin, H., and Bertrand, P. (1993) Structural organization of the iron−sulfur centers in *Synechocystis 6803* photosystem I, *J. Biol. Chem. 268*, 900−908.
81. Metzger, S. U., Cramer, W. A., and Whitmarsh, J. (1997) Critical analysis of the extinction coefficient of chloroplast cytochrome *f*, *Biochim. Biophys. Acta 1319*, 233−241.
82. Bergström, J., and Vanngard, T. (1982) EPR signals and orientation of cytochromes in the spinach chloroplast thylakoid membrane, *Biochim. Biophys. Acta 682*, 452−456.
83. Crowder, M. S., Prince, R. C., and Bearden, A. (1982) Orientation of membrane-bound cytochromes in chloroplasts, detected by low-temperature EPR spectroscopy, *FEBS Lett. 144*, 204−208.
84. Stroebel, D., Choquet, Y., Popot, J. L., and Picot, D. (2003) An atypical haem in the cytochrome b_6f complex, *Nature 426*, 413−418.
85. Poole, C. P., Jr. (1983) *Electron Spin Resonance: A Comprehensive Treatise on Experimental Techniques*, 2nd ed., Dover Publications, Mineola, NY.
86. Kramer, D. M., Roberts, A. G., Muller, F., and Cape, J. (2004) Q-cycle bypass reactions at the Q_o site of the cytochrome bc_1 (and related) complexes, *Methods Enzymol. 382*, 21−45.
87. Gao, X., Wen, X., Yu, C., Esser, L., Tsao, S., Quinn, B., Zhang, L., Yu, L., and Xia, D. (2002) The crystal structure of mitochondrial cytochrome bc_1 in complex with famoxadone: the role of aromatic−aromatic interaction in inhibition, *Biochemistry 41*, 11692−11702.
88. Kim, H., Xia, D., Yu, C. A., Xia, J. Z., Kachurin, A. M., Zhang, L., Yu, L., and Deisenhofer, J. (1998) Inhibitor binding changes domain mobility in the iron−sulfur protein of the mitochondrial bc_1 complex from bovine heart, *Proc. Natl. Acad. Sci. U.S.A. 95*, 8026−8033.
89. Kramer, D. M., and Sacksteder, C. A. (1998) A diffused-optics flash kinetic spectrophotometer (DOFS) for measurements of absorbance changes in intact plants in the steady-state, *Photosynth. Res. 56*, 103−112.
90. Cruz, J. A., Sacksteder, C. A., Kanazawa, A., and Kramer, D. M. (2001) Contribution of electric field ($\Delta\Psi$) to steady-state transthylakoid proton motive force (*pmf*) in vitro and in vivo control

of *pmf* parsing into $\Delta\Psi$ and ΔpH by ionic strength, *Biochemistry 40*, 1226−1237.

91. Bertrand, P., Guigliarelli, B., Gayda, J.-P., Beardwood, P., and Gibson, J. F. (1985) A ligand-field model to describe a new class of 2Fe-2S clusters in proteins and their synthetic analogues, *Biochim. Biophys. Acta 831*, 261−266.
92. Bowman, M. K., Berry, E. A., Roberts, A. G., and Kramer, D. M. (2004) Orientation of the g-tensor axes of the Rieske subunit in the cytochrome bc_1 complex, *Biochemistry 43*, 430−436.
93. Britt, R. D., Sauer, K., Klein, M. P., Knaff, D. B., Kriauciunas, A., Yu, C. A., Yu, L., and Malkin, R. (1991) Electron spin−echo envelope modulation spectroscopy supports the suggested coordination of two histidine ligands to the Rieske Fe−S centers of the cytochrome b_6f complex of spinach and the cytochrome bc_1 complexes of *Rhodospirillum rubrum*, *Rhodobacter sphaeroides R-26*, and bovine heart mitochondria, *Biochemistry 30*, 1892−1901.
94. Cooley, J. W., Roberts, A. G., Bowman, M. K., Kramer, D. M., and Daldal, F. (2004) The raised midpoint potential of the [2Fe2S] cluster of cytochrome bc_1 is mediated by both the Q_o site occupants and the head domain position of the Fe−S protein subunit, *Biochemistry 43*, 2217−2227.
95. Jones, R. W., and Whitmarsh, J. (1988) Inhibition of electron transfer and the electrogenic reaction in the cytochrome *b*/*f* complex by 2-*n*-nonyl-4-hydroxyquinoline *N*-oxide (NQNO) and 2,5-dibromo-3-methyl-6-isopropyl-p-benzoquinone (DBMIB), *Biochim. Biophys. Acta 933*, 258−268.
96. Darrouzet, E., Valkova-Valchanova, M., and Daldal, F. (2002) The [2Fe-2S] cluster E_m as an indicator of the iron−sulfur subunit position in the ubihydroquinone oxidation site of the cytochrome bc_1 complex, *J. Biol. Chem. 277*, 3464−3470.
97. Yan, J., and Cramer, W. A. (2003) Functional insensitivity of the cytochrome b_6f complex to structure changes in the hinge region of the Rieske iron−sulfur protein, *J. Biol. Chem. 278*, 20925−20933.
98. Muster, P., Binder, A., Schneider, K., and Bachofen, R. (1983) Influence of temperature and pH on the growth of the thermophilic cyanobacterium *Mastigocladus laminosus* in continuous culture, *Plant Cell Physiol. 24*, 273−280.

BI049521F